

Biot-JKD model: simulation of 1D transient poroelastic waves with fractional derivatives

Emilie Blanc^a, Guillaume Chiavassa^{b,*}, Bruno Lombard^a

^a*Laboratoire de Mécanique et d'Acoustique, UPR 7051 CNRS, 31 chemin Joseph Aiguier, 13402 Marseille, France*

^b*Centrale Marseille and M2P2, UMR 7340 - CNRS, Technopôle de Chateau-Gombert, 38 rue Frédéric Joliot-Curie, 13451 Marseille, France*

Abstract

A time-domain numerical modeling of Biot poroelastic waves is presented. The viscous dissipation occurring in the pores is described using the dynamic permeability model developed by Johnson-Koplik-Dashen (JKD). Some of the coefficients in the Biot-JKD model are proportional to the square root of the frequency: in the time-domain, these coefficients introduce order 1/2 shifted fractional derivatives involving a convolution product. Based on a diffusive representation, the convolution kernel is replaced by a finite number of memory variables that satisfy local-in-time ordinary differential equations. Thanks to the dispersion relation, the coefficients in the diffusive representation are obtained by performing an optimization procedure in the frequency range of interest. A splitting strategy is then applied numerically: the propagative part of Biot-JKD equations is discretized using a fourth-order ADER scheme on a Cartesian grid, whereas the diffusive part is solved exactly. Comparisons with analytical solutions show the efficiency and the accuracy of this approach.

Keywords: porous media, elastic waves, Biot-JKD model, fractional derivatives, time splitting, finite difference methods, Cartesian grid

2000 MSC: 35L50, 65M06

PACS: 43.20.-Gp, 46.40.-f

*Corresponding author. Tel.: +33 491 05 46 69.

Email addresses: eblanc@lma.cnrs-mrs.fr (Emilie Blanc),
guillaume.chiavassa@centrale-marseille.fr (Guillaume Chiavassa),
lombard@lma.cnrs-mrs.fr (Bruno Lombard)

1. Introduction

Porous media consist of a solid matrix within which fluids can circulate freely. The propagation of waves in these media has many crucial implications in applied mechanics, in situations where materials such as industrial foams, spongy bones [34] and petroleum rocks [3] have to be characterized, for example. The poroelastic model originally developed by Biot in 1956 [1] includes two classical waves (one "fast" compressional wave and one shear wave), in addition to a second "slow" compressional wave, which is highly dependent on the saturating fluid. This slow wave was observed experimentally in 1981 [32], thus confirming the validity of Biot's theory.

Two frequency regimes have to be distinguished when dealing with poroelastic waves. One of the main problems is how to model the dissipation of mechanical energy. In the low-frequency range (LF) [1], the viscous boundary layer that develops in the fluid is large in comparison with the diameter of the pores, and the viscous efforts are proportional to the relative velocity of the motion between the fluid and solid components. In the high-frequency range (HF), modeling the dissipation is a more delicate task: Biot first presented an expression for particular pore geometries [2]. In 1987, Johnson-Koplik-Dashen (JKD) [19] published a general expression for the dissipation in the case of random pores. The viscous efforts depend in this model on the square root of the frequency of the perturbation. When writing the evolution equations in the time domain, time fractional derivatives are introduced, which involves convolution products with singular kernels [26]. Analytical solutions have been derived in simple academic geometries and homogeneous media [13].

Many numerical methods have been developed in the LF regime: see [5] and the introduction to [7] for general reviews. In the HF regime, the fractional derivatives greatly complicate the numerical modeling of the Biot-JKD equations. The past values of the solution are indeed required in order to evaluate these convolution products, which means that the time evolution of the solution must be stored. This of course greatly increases the memory requirements and makes large-scale simulations impossible. To our knowledge, only two approaches to this problem have been proposed so far in the literature. The first approach consisted in discretizing the convolution products [27], and the second one was based on the use of a diffusive representation

of the fractional derivative [25, 36]. In the latter approach, the convolution product is replaced by a continuum of diffusive variables - or memory variables - satisfying local differential equations [17]. This continuum is then discretized using appropriate quadrature formulas, resulting in the Biot-DA (diffusive approximation) model.

However, the diffusive approximation proposed in [25] has three major drawbacks. First, the quadrature formulas make the convergence towards the original fractional operator very slow. Secondly, in the case of small frequencies, the Biot-DA model does not converge towards the Biot-LF model. Lastly, the number of memory variables required is not specified. The aim of the present study is therefore to develop a new diffusive approximation method in which these drawbacks do not arise. Since it is proposed here to focus on the discretization of the fractional derivatives, we will deal only with the 1-D equations of evolution in homogeneous media, so that the shear wave will not be considered. However, the strategy proposed here can be extended quite straightforwardly to 2D and 3D geometries, as discussed below.

This paper is organized as follows. The original Biot-JKD model is briefly outlined in section 2 and the principles underlying the diffusive representation of fractional derivatives are described. The decrease of energy and the dispersion analysis are addressed. In section 3, the method used to discretize the diffusive model is presented: the diffusive approximation thus obtained is easily treatable by computers. Following a similar approach than in viscoelasticity [15], the coefficients of the model are determined using an optimization procedure in the frequency range of interest, giving an optimum number of additional computational arrays. The numerical modeling is addressed in section 4, where the equations of evolution are split into two parts: a propagative part, which is discretized using a fourth-order scheme for hyperbolic equations, and a diffusive part, which is solved exactly. Some numerical experiments performed with realistic values of the physical parameters are presented in section 5. In section 6, a conclusion is drawn and some futures lines of research are given.

2. Physical modeling

2.1. Biot model

The Biot model describes the propagation of mechanical waves in a macroscopic porous medium consisting of a solid matrix saturated with a fluid circulating freely through the pores [1, 3, 4]. It is assumed that

- the wavelengths are large in comparison with the diameter of the pores;
- the amplitude of the perturbations is small;
- the elastic and isotropic matrix is completely saturated with a single fluid phase;
- the thermo-mechanical effects are neglected.

This model involves 10 physical parameters: the density ρ_f and the dynamic viscosity η of the fluid; the density ρ_s and the shear modulus μ of the elastic skeleton; the porosity $0 < \phi < 1$, the tortuosity $a \geq 1$, the absolute permeability at null frequency κ , the Lamé coefficient λ_f and the two Biot's coefficients β and m of the saturated matrix. The following notations are introduced

$$\begin{aligned} \rho_w &= \frac{a}{\phi} \rho_f, \quad \rho = \phi \rho_f + (1 - \phi) \rho_s, \quad \chi = \rho \rho_w - \rho_f^2 > 0, \\ \lambda_0 &= \lambda_f - m \beta^2, \quad C = \lambda_0 + 2 \mu > 0. \end{aligned} \quad (1)$$

Taking u_s and u_f to denote the solid and fluid displacements, the unknowns in 1D are the elastic velocity $v_s = \frac{\partial u_s}{\partial t}$, the filtration velocity $w = \frac{\partial \mathcal{W}}{\partial t} = \phi \frac{\partial}{\partial t} (u_f - u_s)$, the elastic stress σ , and the acoustic pressure p . The constitutive laws are

$$\begin{cases} \sigma = (\lambda_f + 2 \mu) \varepsilon - m \beta \xi, & (2a) \\ p = m (-\beta \varepsilon + \xi), & (2b) \end{cases}$$

where $\varepsilon = \frac{\partial u_s}{\partial x}$ is the strain and $\xi = -\frac{\partial \mathcal{W}}{\partial x}$ is the rate of fluid change. On the other hand, the conservation of momentum yields

$$\begin{cases} \rho \frac{\partial v_s}{\partial t} + \rho_f \frac{\partial w}{\partial t} = \frac{\partial \sigma}{\partial x} + f_b, & (3a) \\ \rho_s \frac{\partial v_s}{\partial t} + \rho_w \frac{\partial w}{\partial t} + \frac{\eta}{\kappa} F * w = -\frac{\partial p}{\partial x} + f_f, & (3b) \end{cases}$$

where $*$ is the convolution product in time; f_b and f_f are the body force for an unit volume of the bulk material and the pore fluid, respectively. The equation (3b) is a generalized Darcy law. The quantity $F * w$ denotes the viscous dissipation induced by the relative motion between the fluid and the elastic skeleton.

2.2. High frequency dissipation: the JKD model

The frontier between the low-frequency range (LF) and the high-frequency range (HF) is reached when the viscous efforts and the inertial effects are similar. The transition frequency is given by [1, 3]

$$f_c = \frac{\eta \phi}{2 \pi a \kappa \rho_f} = \frac{\omega_c}{2 \pi}. \quad (4)$$

In LF, the flow in the pores is of the Poiseuille type, and dissipation efforts in (3b) are given by

$$F(t) = \delta(t) \iff F(t) * w(x, t) = w(x, t), \quad (5)$$

where δ is the Dirac distribution. In HF, the width of the viscous boundary-layer is small in comparison with the size of the pores, and modeling the dissipation process is a more complex task. Here we adopt the widely-used model proposed by Johnson-Koplik-Dashen (JKD) in 1987, which is valid for random networks of pores with constant radii [19]. The only additional parameter is the viscous characteristic length Λ . We take

$$P = \frac{4 a \kappa}{\phi \Lambda^2}, \quad \Omega = \frac{\omega_c}{P} = \frac{\eta \phi^2 \Lambda^2}{4 a^2 \kappa^2 \rho_f}, \quad (6)$$

where P is the Pride number (typically $P \approx 1/2$). Based on the Fourier transform in time, $\widehat{F}(\omega) = \int_{\mathbb{R}} F(t) e^{-i\omega t} dt$, the frequency correction given by the JKD model can be written

$$\begin{aligned} \widehat{F}(\omega) &= \left(1 + i\omega \frac{4 a^2 \kappa^2 \rho_f}{\eta \Lambda^2 \phi^2} \right)^{1/2}, \\ &= \left(1 + iP \frac{\omega}{\omega_c} \right)^{1/2}, \\ &= \frac{1}{\sqrt{\Omega}} (\Omega + i\omega)^{1/2}. \end{aligned} \quad (7)$$

This correction is the simplest function satisfying the LF and HF limits of the dynamic permeability [19]. Therefore, the term $F(t) * w(x, t)$ involved in (3b) is

$$\begin{aligned} F(t) * w(x, t) &= \mathcal{F}^{-1} \left(\frac{1}{\sqrt{\Omega}} (\Omega + i\omega)^{1/2} \widehat{w}(x, \omega) \right), \\ &= \frac{1}{\sqrt{\Omega}} (D + \Omega)^{1/2} w(x, t). \end{aligned} \quad (8)$$

The operator $D^{1/2}$ is a shifted order 1/2 time fractional derivative, generalizing the usual derivative characterized by $\frac{\partial w}{\partial t} = \mathcal{F}^{-1}(i\omega \widehat{w}(\omega))$. The notation $(D + \Omega)^{1/2}$ accounts for the shift Ω in (8).

2.3. The Biot-JKD equations of evolution

Based on (2), (3) and (8), the Biot-JKD equations can be written

$$\left\{ \begin{array}{l} \rho \frac{\partial v_s}{\partial t} + \rho_f \frac{\partial w}{\partial t} = \frac{\partial \sigma}{\partial x} + f_b, \end{array} \right. \quad (9a)$$

$$\left\{ \begin{array}{l} \rho_f \frac{\partial v_s}{\partial t} + \rho_w \frac{\partial w}{\partial t} + \frac{\eta}{\kappa} \frac{1}{\sqrt{\Omega}} (D + \Omega)^{1/2} w = -\frac{\partial p}{\partial x} + f_f, \end{array} \right. \quad (9b)$$

$$\left\{ \begin{array}{l} \sigma = (\lambda_f + 2\mu) \varepsilon - m \beta \xi, \end{array} \right. \quad (9c)$$

$$\left\{ \begin{array}{l} p = m(-\beta \varepsilon + \xi). \end{array} \right. \quad (9d)$$

We rearrange this system by separating $\frac{\partial v_s}{\partial t}$ and $\frac{\partial w}{\partial t}$ in (9a) and (9b) and using the definitions of ε and ξ . Taking

$$\gamma = \frac{\eta}{\kappa} \frac{\rho}{\chi} \frac{1}{\sqrt{\Omega}}, \quad (10)$$

one obtains the following system of equations of evolution

$$\left\{ \begin{array}{l} \frac{\partial v_s}{\partial t} - \frac{\rho_w}{\chi} \frac{\partial \sigma}{\partial x} - \frac{\rho_f}{\chi} \frac{\partial p}{\partial x} = \frac{\rho_f}{\rho} \gamma (D + \Omega)^{1/2} w + f_{v_s}, \end{array} \right. \quad (11a)$$

$$\left\{ \begin{array}{l} \frac{\partial w}{\partial t} + \frac{\rho_f}{\chi} \frac{\partial \sigma}{\partial x} + \frac{\rho}{\chi} \frac{\partial p}{\partial x} = -\gamma (D + \Omega)^{1/2} w + f_w, \end{array} \right. \quad (11b)$$

$$\left\{ \begin{array}{l} \frac{\partial \sigma}{\partial t} - (\lambda_f + 2\mu) \frac{\partial v_s}{\partial x} - m \beta \frac{\partial w}{\partial x} = f_\sigma, \end{array} \right. \quad (11c)$$

$$\left\{ \begin{array}{l} \frac{\partial p}{\partial t} + m \beta \frac{\partial v_s}{\partial x} + m \frac{\partial w}{\partial x} = f_p, \end{array} \right. \quad (11d)$$

with $f_{v_s} = (\rho_w f_b - \rho_f f_f) / \chi$ and $f_w = (\rho f_f - \rho_f f_b) / \chi$. Terms f_σ and f_p have also been added to the derivatives of constitutive laws to simulate sources of mass.

2.4. The diffusive representation

Taking

$$D_{\Omega}w(x, t) = \frac{\partial w}{\partial t} + \Omega w, \quad (12)$$

the shifted fractional derivative (8) can be written [10]

$$(D + \Omega)^{1/2}w(x, t) = \frac{1}{\sqrt{\pi}} \int_0^t \frac{e^{-\Omega(t-\tau)}}{\sqrt{t-\tau}} D_{\Omega}w(x, \tau) d\tau. \quad (13)$$

The operator $(D + \Omega)^{1/2}$ is not local in time and involves the entire time history of w . As we will see in section 3, a different way of writing this derivative is more convenient for numerical evaluation. Based on Euler's Γ function, the diffusive representation of the totally monotone function $\frac{1}{\sqrt{t}}$ [9, 17, 18, 35] is

$$\frac{1}{\sqrt{t}} = \frac{1}{\sqrt{\pi}} \int_0^{\infty} \frac{1}{\sqrt{\theta}} e^{-\theta t} d\theta. \quad (14)$$

Substituting (14) into (13) gives

$$\begin{aligned} (D + \Omega)^{1/2}w(x, t) &= \frac{1}{\pi} \int_0^t \int_0^{\infty} \frac{1}{\sqrt{\theta}} e^{-\theta(t-\tau)} e^{-\Omega(t-\tau)} D_{\Omega}w(x, \tau) d\theta d\tau, \\ &= \frac{1}{\pi} \int_0^{\infty} \frac{1}{\sqrt{\theta}} \psi(x, \theta, t) d\theta, \end{aligned} \quad (15)$$

where the diffusive variable is defined as

$$\psi(x, \theta, t) = \int_0^t e^{-(\theta+\Omega)(t-\tau)} D_{\Omega}w(x, \tau) d\tau. \quad (16)$$

For the sake of clarity, the dependence on Ω and w is omitted in ψ . From (16), it follows that the diffusive variable ψ satisfies the ordinary differential equation

$$\begin{cases} \frac{\partial \psi}{\partial t} = -(\theta + \Omega) \psi + D_{\Omega}w, \\ \psi(x, \theta, 0) = 0. \end{cases} \quad (17)$$

The diffusive representation therefore transforms a non-local problem (13) into a continuum of local problems (17). It should be emphasized at this point that no approximations have been made up to now. The computational advantages of the diffusive representation will be seen in sections 3 and 5, where the discretization of (15) and (17) will yield a tractable formulation.

2.5. Energy of Biot-JKD

Now, we express the energy of the Biot-JKD model 9). This result generalizes the analysis performed in the LF range in [12].

Proposition 1. *Let*

$$E = E_1 + E_2 + E_3,$$

with

$$\begin{aligned} E_1 &= \frac{1}{2} \int_{\mathbb{R}} (\rho v^2 + \rho_w w^2 + 2 \rho_f v w) dx, \\ E_2 &= \frac{1}{2} \int_{\mathbb{R}} \left(\frac{1}{C} (\sigma + \beta p)^2 + \frac{1}{m} p^2 \right) dx, \\ E_3 &= \frac{1}{2} \int_{\mathbb{R}} \int_{\theta \in \mathbb{R}^+} \frac{\eta}{\kappa} \frac{1}{\pi} \frac{1}{\sqrt{\Omega \theta}} \frac{1}{\theta + 2\Omega} (w - \psi)^2 d\theta dx. \end{aligned} \quad (18)$$

Then E is an energy which satisfies

$$\frac{dE}{dt} = - \int_{\mathbb{R}} \int_{\theta \in \mathbb{R}^+} \frac{\eta}{\kappa} \frac{1}{\pi} \frac{1}{\sqrt{\Omega \theta}} \frac{1}{\theta + 2\Omega} (\Omega w^2 + (\theta + \Omega) \psi^2) d\theta dx \leq 0. \quad (19)$$

Proposition 1 is proven in appendix 1. It calls for the following comments:

- the Biot-JKD model is well-posed;
- when the viscosity of the saturating fluid is neglected ($\eta = 0$), the energy of the system is conserved;
- the terms in (18) have a clearly physical significance: E_1 is the kinetic energy, and E_2 is the potential energy. The term E_3 corresponds to the kinetic energy resulting from the filtration velocity.

2.6. Dispersion analysis

Injecting a mode $e^{i(\omega t - kx)}$ in (11) gives the dispersion relation between the angular frequency ω and the wavenumber k . Taking

$$\begin{cases} D_4 &= m(\lambda_0 + 2\mu), \\ D_2(\omega) &= -((\lambda_f + 2\mu)\rho_w + m(\rho - 2\rho_f\beta))\omega^2 + i\omega \frac{\eta}{\kappa} \widehat{F}(\omega)(\lambda_f + 2\mu), \\ D_0(\omega) &= \chi\omega^4 - i\omega^3 \frac{\eta}{\kappa} \rho \widehat{F}(\omega). \end{cases} \quad (20)$$

the dispersion relation takes the form

$$D_e(k, \omega) = D_4 k^4 + D_2(\omega) k^2 + D_0(\omega) = 0. \quad (21)$$

Expressions (20)-(21) are valid in the case of both the Biot-LF and Biot-JKD models with the frequency correction defined by

$$\widehat{F}(\omega) = \begin{cases} \widehat{F}_{LF}(\omega) = 1 & \text{Biot-LF,} \\ \widehat{F}_{JKD}(\omega) = \frac{1}{\sqrt{\Omega}} (\Omega + i\omega)^{1/2} & \text{Biot-JKD.} \end{cases} \quad (22a)$$

$$(22b)$$

The solutions k_{pf} and k_{ps} of (21) give the phase velocities $c_{pf} = \omega/\Re(k_{pf})$ of the fast wave and $c_{ps} = \omega/\Re(k_{ps})$ of the slow wave, with $0 < c_{ps} < c_{pf}$. The attenuations $\alpha_{pf} = -\Im(k_{pf})$ and $\alpha_{ps} = -\Im(k_{ps})$ can also be deduced. Both the phase velocities and the attenuations of Biot-LF and Biot-JKD are strictly increasing functions of the frequency. The high frequency limits of fast and slow phase velocities, c_{pf}^∞ and c_{ps}^∞ , which are obtained by diagonalizing the left-hand side of system (11), satisfy the relation

$$\chi c^4 - ((\lambda_f + 2\mu)\rho_w + m(\rho - 2\rho_f\beta))c^2 + m(\lambda_0 + 2\mu) = 0. \quad (23)$$

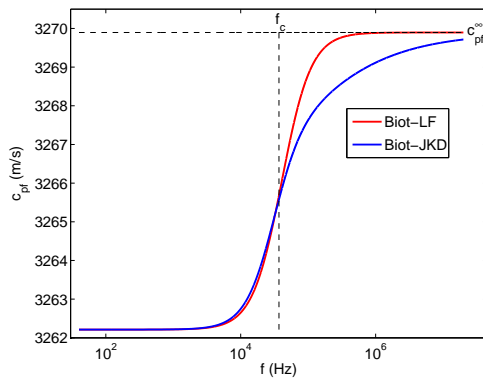
Figure 1 shows the dispersion curves corresponding to the Biot-LF and Biot-JKD models. The physical parameters are those used in the numerical experiments presented in section 5. Note that the scales are radically different in the case of fast and slow waves. The following properties can be observed:

- when $f < f_c$, the Biot-JKD and Biot-LF dispersion curves are very similar as might be expected, since $\lim_{\omega \rightarrow 0} \widehat{F}_{JKD}(\omega) = 1$;
- the fast wave is almost not affected by the frequency correction $\widehat{F}(\omega)$ while the slow wave is greatly affected;
- when $f \ll f_c$, the slow wave degenerates to a diffusion process and is characterized by $\Re(k_{ps}) = \Im(k_{ps})$. When $f > f_c$, the slow wave propagates but is greatly attenuated.

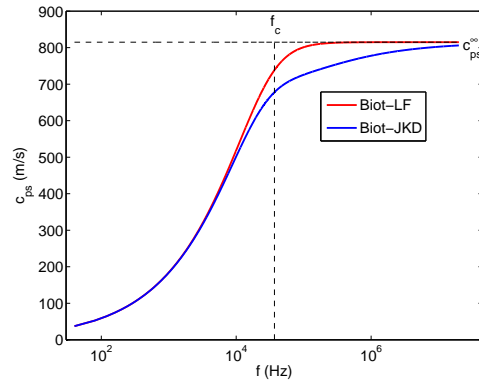
3. The Biot-DA (diffusive approximation) model

The aim of this section is to approximate the Biot-JKD model, using a numerically tractable approach. For this purpose, we follow a diffusive representation of fractional derivatives, initially proposed in [25].

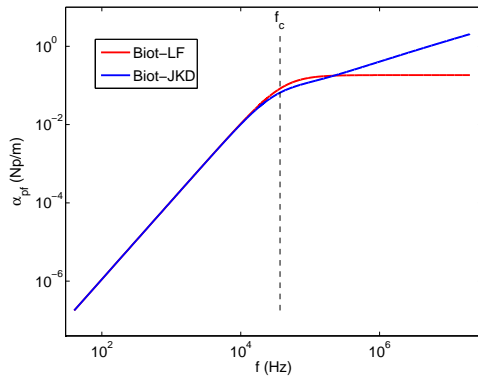
phase velocity of the fast wave



phase velocity of the slow wave



attenuation of the fast wave



attenuation of the slow wave

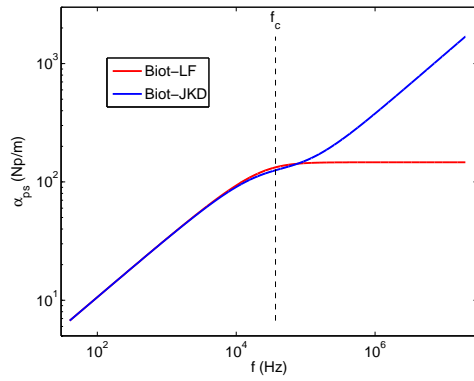


Figure 1: Dispersion curves: comparison between Biot-LF and Biot-JKD.

3.1. The Biot-DA first-order system

Using a quadrature formula on N points, with weights a_ℓ and abscissa $\theta_\ell > 0$, the diffusive representation (15) can be approximated by

$$\begin{aligned}
(D + \Omega)^{1/2} w(x, t) &= \frac{1}{\pi} \int_0^\infty \frac{1}{\sqrt{\theta}} \psi(x, t, \theta) d\theta, \\
&\simeq \sum_{\ell=1}^N a_\ell \psi(x, t, \theta_\ell), \\
&\equiv \sum_{\ell=1}^N a_\ell \psi_\ell(x, t).
\end{aligned} \tag{24}$$

From (17), the N diffusive variables ψ_ℓ satisfy the ordinary differential equations

$$\begin{cases} \frac{\partial \psi_\ell}{\partial t} = -(\theta_\ell + \Omega) \psi_\ell + D_\Omega w, \\ \psi_\ell(x, 0) = 0. \end{cases} \tag{25}$$

The fractional derivatives are replaced by their diffusive approximation (24) in the JKD model (11). Upon adding the equations (25) and performing some straightforward operations, the Biot-DA system is written as a first-order system in time and space

$$\begin{cases} \frac{\partial v_s}{\partial t} - \frac{\rho_w}{\chi} \frac{\partial \sigma}{\partial x} - \frac{\rho_f}{\chi} \frac{\partial p}{\partial x} = \frac{\rho_f}{\rho} \gamma \sum_{\ell=1}^N a_\ell \psi_\ell + f_{v_s}, \\ \frac{\partial w}{\partial t} + \frac{\rho_f}{\chi} \frac{\partial \sigma}{\partial x} + \frac{\rho}{\chi} \frac{\partial p}{\partial x} = -\gamma \sum_{\ell=1}^N a_\ell \psi_\ell + f_w, \\ \frac{\partial \sigma}{\partial t} - (\lambda_f + 2\mu) \frac{\partial v_s}{\partial x} - m\beta \frac{\partial w}{\partial x} = f_\sigma, \\ \frac{\partial p}{\partial t} + m\beta \frac{\partial v_s}{\partial x} + m \frac{\partial w}{\partial x} = f_p, \\ \frac{\partial \psi_j}{\partial t} + \frac{\rho_f}{\chi} \frac{\partial \sigma}{\partial x} + \frac{\rho}{\chi} \frac{\partial p}{\partial x} = \Omega w - \gamma \sum_{\ell=1}^N a_\ell \psi_\ell - (\theta_j + \Omega) \psi_j + f_w, \quad j = 1, \dots, N. \end{cases} \tag{26}$$

Taking the vector of unknowns

$$\mathbf{U} = (v_s, w, \sigma, p, \psi_1, \dots, \psi_N)^T \tag{27}$$

and the source vector

$$\mathbf{F} = (f_{v_s}, f_w, f_\sigma, f_p, f_w, \dots, f_w)^T, \quad (28)$$

the system (26) can be written

$$\frac{\partial \mathbf{U}}{\partial t} + \mathbf{A} \frac{\partial \mathbf{U}}{\partial x} = -\mathbf{S} \mathbf{U} + \mathbf{F}, \quad (29)$$

where \mathbf{A} is the $(N + 4)^2$ propagation matrix

$$\mathbf{A} = \left(\begin{array}{cccc|ccc} 0 & 0 & -\frac{\rho_w}{\chi} & -\frac{\rho_f}{\chi} & 0 & \dots & 0 \\ 0 & 0 & \frac{\rho_f}{\chi} & \frac{\rho}{\chi} & \vdots & \dots & \vdots \\ -(\lambda_f + 2\mu) & -m\beta & 0 & 0 & \vdots & \dots & \vdots \\ m\beta & m & 0 & 0 & 0 & \dots & 0 \\ \hline 0 & 0 & \frac{\rho_f}{\chi} & \frac{\rho}{\chi} & 0 & \dots & 0 \\ \vdots & \vdots & \vdots & \vdots & \vdots & \dots & \vdots \\ 0 & 0 & \frac{\rho_f}{\chi} & \frac{\rho}{\chi} & 0 & \dots & 0 \end{array} \right), \quad (30)$$

and \mathbf{S} is the $(N + 4)^2$ dissipation matrix

$$\mathbf{S} = \left(\begin{array}{cccc|cccc} 0 & 0 & 0 & 0 & -\frac{\rho_f}{\rho} \gamma a_1 & -\frac{\rho_f}{\rho} \gamma a_2 & \dots & -\frac{\rho_f}{\rho} \gamma a_N \\ 0 & 0 & 0 & 0 & \gamma a_1 & \gamma a_2 & \dots & \gamma a_N \\ 0 & 0 & 0 & 0 & 0 & \dots & \dots & 0 \\ 0 & 0 & 0 & 0 & 0 & \dots & \dots & 0 \\ \hline 0 & -\Omega & 0 & 0 & \gamma a_1 + (\theta_1 + \Omega) & \gamma a_2 & \dots & \gamma a_N \\ 0 & -\Omega & 0 & 0 & \gamma a_1 & \gamma a_2 + (\theta_2 + \Omega) & \dots & \gamma a_N \\ \vdots & \vdots & \vdots & \vdots & \vdots & \vdots & \ddots & \vdots \\ 0 & -\Omega & 0 & 0 & \gamma a_1 & \gamma a_2 & \dots & \gamma a_N + (\theta_N + \Omega) \end{array} \right). \quad (31)$$

The size of the system increases linearly with the number N of diffusive variables.

3.2. Properties

Four properties of system (29) are specified:

- the eigenvalues of \mathbf{A} (30) are real: 0 with multiplicity N , $\pm c_{pf}^\infty$ and $\pm c_{ps}^\infty$, where the latter satisfies (23). The system (29) is therefore hyperbolic;
- since the eigenvalues and eigenvectors do not depend on the diffusive coefficients, they are the same in both the Biot-DA and Biot-LF or Biot-JKD models. This is not so in the case of the method presented in [27], where the propagation matrix is modified to account for the fractional derivative;
- the dispersion analysis is obtained in the case of the Biot-DA model by replacing \widehat{F} by

$$\widehat{F}_{DA}(\omega) = \frac{\Omega + i\omega}{\sqrt{\Omega}} \sum_{\ell=1}^N \frac{a_\ell}{\theta_\ell + \Omega + i\omega} \quad (32)$$

in equations (20)-(21);

- in line with proposition 1, an energy analysis of (26) is performed.

Proposition 2. *Let*

$$E = E_1 + E_2 + E_3,$$

with

$$\begin{aligned} E_1 &= \frac{1}{2} \int_{\mathbb{R}} (\rho v^2 + \rho_w w^2 + 2\rho_f v w) dx, \\ E_2 &= \frac{1}{2} \int_{\mathbb{R}} \left(\frac{1}{C} (\sigma + \beta p)^2 + \frac{1}{m} p^2 \right) dx, \\ E_3 &= \frac{1}{2} \int_{\mathbb{R}} \sum_{\ell=1}^N \frac{\eta}{\kappa} \frac{1}{\sqrt{\Omega}} \frac{a_\ell}{\theta_\ell + 2\Omega} (w - \psi_\ell)^2 dx. \end{aligned} \quad (33)$$

Then E satisfies

$$\frac{dE}{dt} = - \int_{\mathbb{R}} \sum_{\ell=1}^N \frac{\eta}{\kappa} \frac{1}{\sqrt{\Omega}} \frac{a_\ell}{\theta_\ell + 2\Omega} (\Omega w^2 + (\theta_\ell + \Omega) \psi_\ell^2) dx. \quad (34)$$

Since the proof is very similar in this case, it will not be repeated. The terms E_1 and E_2 are the same in both the Biot-DA and Biot-JKD models, whereas E_3 and the time evolution of E differ; in Biot-DA, the sign depends on the coefficients introduced into the diffusive approximation. The abscissas θ_ℓ of the quadrature formula are positive, but no sign criterion is given a priori for the weights a_ℓ . E therefore cannot be said to be a decreasing energy, except in the obvious case where all the a_ℓ are positive.

3.3. Determination of the Biot-DA parameters

The a_ℓ and θ_ℓ in (24) now have to be determined. In [25], the authors used a general Laguerre quadrature formulas. We have tried using this approach, but it gave poor results. Very large numbers of diffusive variables were required to approximate the Biot-JKD model accurately, resulting in a huge computational cost. In addition, the Biot-DA model based on Laguerre functions does not converge by construction towards Biot-LF when the frequency tends towards 0, which is neither satisfactory nor physically realistic. Lastly, the involved coefficients do not depend on the physical factors (parameters, source) involved, which partly explains the above two weaknesses.

A different method of determining the $2N$ coefficients a_ℓ and θ_ℓ in the diffusive approximation (26) is therefore used, in order to approach $\widehat{F}_{JKD}(\omega)$ (22) by $\widehat{F}_{DA}(\omega)$ (32) in a given frequency range of interest. Let $Q(\omega)$ be the optimized quantity and $Q_{ref}(\omega)$ be the desired quantity

$$\begin{cases} Q(\omega) = \frac{\widehat{F}_{DA}(\omega)}{\widehat{F}_{JKD}(\omega)} = \sum_{\ell=1}^N a_\ell \frac{(\Omega + i\omega)^{1/2}}{\theta_\ell + \Omega + i\omega} = \sum_{\ell=1}^N a_\ell q_\ell(\omega), & (35a) \\ Q_{ref}(\omega) = 1. & (35b) \end{cases}$$

We implement a linear optimization procedure [11, 16, 24] in order to minimize the distance between $Q(\omega)$ and $Q_{ref}(\omega)$ in the interval $[\omega_{min}, \omega_{max}]$ centered on $\omega_0 = 2\pi f_0$, where f_0 is the central frequency of the source. The abscissas θ_ℓ are fixed and distributed linearly on a logarithmic scale

$$\theta_\ell = \omega_{min} \left(\frac{\omega_{max}}{\omega_{min}} \right)^{\frac{\ell-1}{N-1}}, \quad \ell = 1, \dots, N. \quad (36)$$

The weights a_ℓ are obtained by solving the system

$$\sum_{\ell=1}^N a_\ell q_\ell(\tilde{\omega}_k) = 1, \quad k = 1, \dots, K, \quad (37)$$

where the $\tilde{\omega}_k$ are also distributed linearly on a logarithmic scale of K points

$$\tilde{\omega}_k = \omega_{min} \left(\frac{\omega_{max}}{\omega_{min}} \right)^{\frac{k-1}{K-1}}, \quad k = 1, \dots, K. \quad (38)$$

Since the $q_\ell(\omega)$ are complex functions, optimization is performed simultaneously on the real and imaginary parts

$$\begin{cases} \sum_{\ell=1}^N a_\ell \Re(q_\ell(\tilde{\omega}_k)) = 1, \\ \sum_{\ell=1}^N a_\ell \Im(q_\ell(\tilde{\omega}_k)) = 0, \end{cases} \quad k = 1, \dots, K. \quad (39)$$

A square system is obtained when $2K = N$, whereas $2K > N$ yields an overdetermined system, which can be solved by writing normal equations

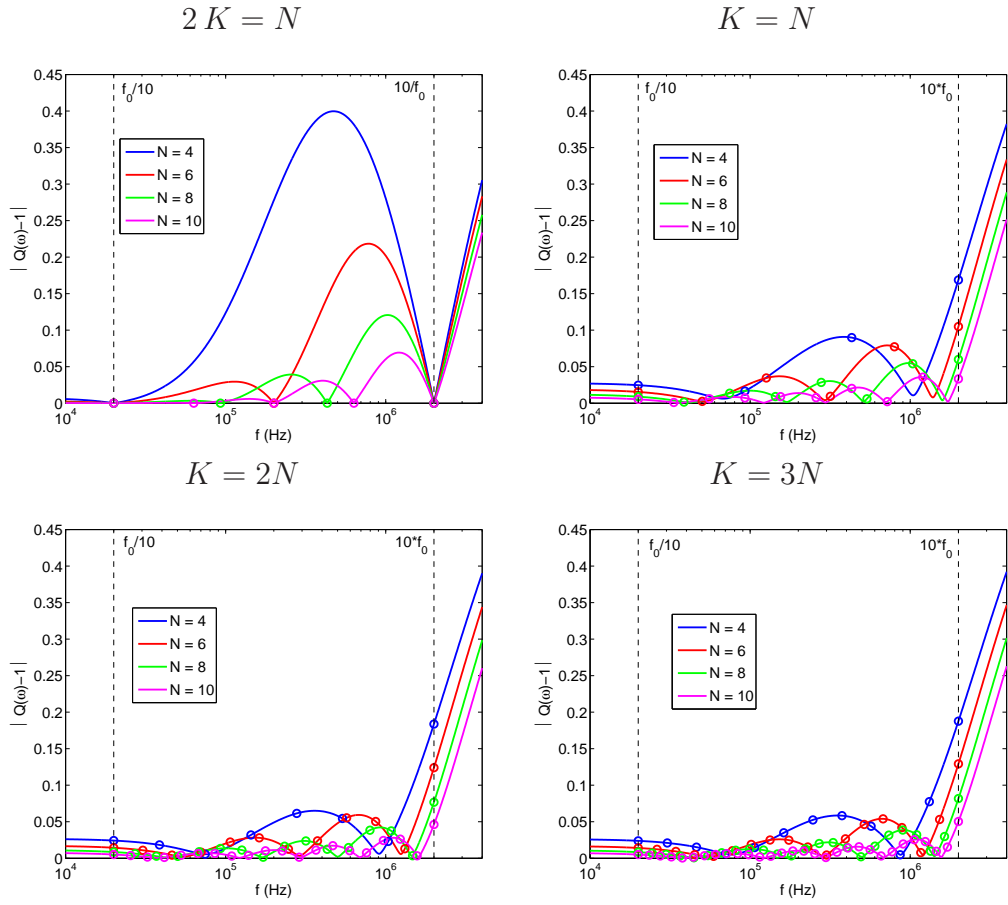


Figure 2: Relative error $|Q(\omega) - 1|$ in (35b) in the case of various values of (K, N) .

[14]. For practical purposes, we use $\omega_{min} = \omega_0/10$ and $\omega_{max} = 10\omega_0$, as in [24].

Figure 2 illustrates the influence of N and K on the accuracy of the optimization procedure. As can be observed in this figure, the errors are smaller with the overdetermined system ($K = N, 2N, 3N$) than with the square one. However, increasing the size of the system does not really improve the accuracy. In what follows, we will therefore always use the values $K = N$. The influence of the number of diffusive variables on the physical properties of the system is presented in figure 3. We focus here on the slow wave, since it is more sensitive to the frequency correction. As was to be expected, the accuracy of the approximation of the Biot-JKD phase velocity and attenuation given by the Biot-DA model increases with N .

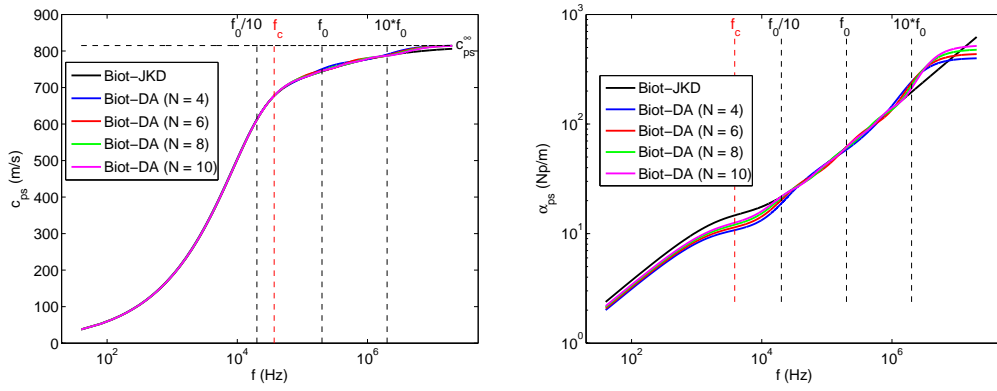


Figure 3: Phase velocity c_{ps} (left) and attenuation α_{ps} (right) of the slow wave obtained with the Biot-DA model, in terms of the number of diffusive variables.

To determine N in terms of the required accuracy, $\varepsilon_m = \|Q(\omega) - 1\|_{L_2}$ is measured in the frequency range of interest $[f_0/10, 10f_0]$. This norm amounts to the relative error between $\widehat{F}_{DA}(\omega)$ and $\widehat{F}_{JKD}(\omega)$. With $N \leq 20$, this error is proportional to N^{-1} , as can be seen from figure 4-(a). At larger values of N , the system is poorly conditioned and the order of convergence deteriorates (not shown here); in practice, this is not penalizing, however, since large values of N are of no use. An example of the parametric determination of N in terms of the frequency range and the desired accuracy is also given in figure 4-(b). In the following numerical tests, $N = 6$ variables are used, giving the modeling error $\varepsilon_m \simeq 5.5\%$.

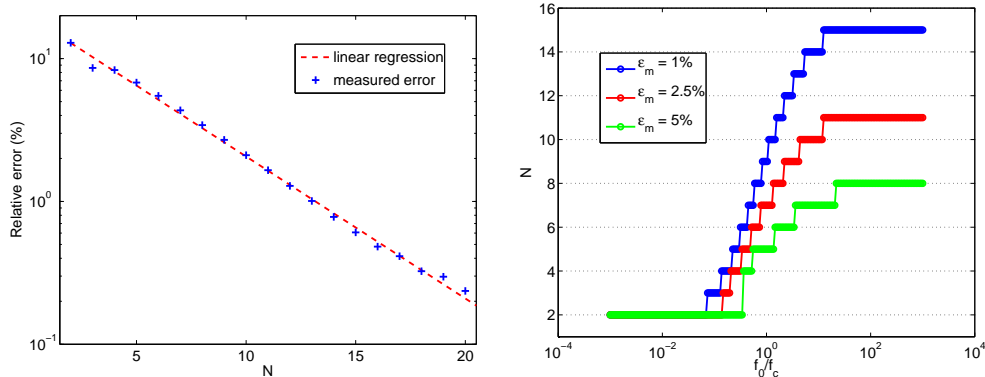


Figure 4: Determining the number of diffusive variables N . Left: relative error ε_m in terms of the number of N ; the dashed line is proportional to N^{-1} . Right: required value of N in terms of f_0/f_c and the required accuracy ε_m (b).

Lastly, the sign of weights a_ℓ was examined in a large number of configurations. In each case, some negative values were obtained with the linear optimization process (39). As stated in proposition 2, the well-posedness of Biot-DA could not therefore be proved. A nonlinear optimization procedure with a positivity constraint was then applied [31], but almost all the a_ℓ obtained were equal to zero. In the numerical experiments, the negativity of some a_ℓ has never raised any problems. This question is addressed in detail at the end of section 5.2.

4. Numerical modeling

4.1. Splitting

In order to integrate the Biot-DA system (29), a uniform grid is introduced, with mesh size Δx and time step Δt . The approximation of the exact solution $\mathbf{U}(x_j = j \Delta x, t_n = n \Delta t)$ is denoted by \mathbf{U}_j^n . If an unsplit integration of (29) is performed, Von-Neumann analysis typically yields the stability condition

$$\Delta t \leq \min \left(\Upsilon \frac{\Delta x}{c_{pf}^\infty}, \frac{2}{R(\mathbf{S})} \right), \quad (40)$$

where $R(\mathbf{S})$ is the spectral radius of \mathbf{S} , and $\Upsilon > 0$ depends on the numerical scheme. We have no theoretical estimate of $R(\mathbf{S})$, but numerical studies have

shown that this value is similar to that of the spectral radius in LF: $\frac{\eta}{\kappa} \frac{\rho}{\chi}$, which can be very large [7]. The time step can therefore be highly penalized in this case (40).

A more efficient strategy is adopted here, which consists in splitting the original system (29) into a propagative part and a diffusive part (42)

$$\left\{ \begin{array}{l} \frac{\partial \mathbf{U}}{\partial t} + \mathbf{A} \frac{\partial \mathbf{U}}{\partial x} = 0, \\ \frac{\partial \mathbf{U}}{\partial t} = -\mathbf{S} \mathbf{U}. \end{array} \right. \quad (41)$$

$$\left\{ \begin{array}{l} \frac{\partial \mathbf{U}}{\partial t} = -\mathbf{S} \mathbf{U}. \end{array} \right. \quad (42)$$

For the sake of simplicity, the source term \mathbf{F} has been omitted here. The discrete operators associated with steps (41) and (42) are denoted by \mathbf{H}_a and \mathbf{H}_b , respectively. The second-order Strang splitting [22] is then used to integrate (29) between t_n and t_{n+1} , giving the time-marching

$$\begin{aligned} \bullet \quad \mathbf{U}_j^{(1)} &= \mathbf{H}_b\left(\frac{\Delta t}{2}\right) \mathbf{U}_j^n, \\ \bullet \quad \mathbf{U}_j^{(2)} &= \mathbf{H}_a(\Delta t) \mathbf{U}_j^{(1)}, \\ \bullet \quad \mathbf{U}_j^{n+1} &= \mathbf{H}_b\left(\frac{\Delta t}{2}\right) \mathbf{U}_j^{(2)}. \end{aligned} \quad (43)$$

The discrete operator \mathbf{H}_a associated with the propagative part (41) is an ADER 4 (Arbitrary DERivatives) scheme [33]. This scheme is fourth-order accurate in space and time, is dispersive of order 4 and dissipative of order 6, and has a stability limit $\Upsilon = 1$. On Cartesian grids, ADER 4 amounts to a fourth-order Lax-Wendroff scheme, and can be written

$$\left\{ \begin{array}{l} \mathbf{H}_a(\Delta t) \mathbf{U}_j^{(1)} = \mathbf{U}_j^{(1)} - \sum_{s=-2}^{+2} \mathbf{C}_s \mathbf{U}_{j+s}^{(1)}, \\ \mathbf{C}_s = - \sum_{m=1}^4 \gamma_{m,s} \left(-\mathbf{A} \frac{\Delta t}{\Delta x} \right)^m, \end{array} \right. \quad (44)$$

where the coefficients $\gamma_{m,s}$ are given in table 1.

Since the physical parameters do not vary with time, the diffusive part (42) can be solved exactly. This gives

$$\mathbf{H}_b\left(\frac{\Delta t}{2}\right) \mathbf{U}_j = e^{-\frac{\Delta t}{2} \mathbf{S}} \mathbf{U}_j. \quad (45)$$

$\gamma_{m,s}$	$m = 1$	$m = 2$	$m = 3$	$m = 4$
$s = -2$	1/12	1/24	-1/12	-1/24
$s = -1$	-2/3	-2/3	1/6	1/6
$s = 0$	0	5/4	0	-1/4
$s = +1$	2/3	-2/3	-1/6	1/6
$s = +2$	-1/12	1/24	1/12	-1/24

Table 1: Coefficients of the ADER 4 scheme.

The matrix $e^{-\frac{\Delta t}{2}\mathbf{S}}$ is computed numerically using the (r/q) Padé approximation in the "scaling and squaring method" [28], which is given by the expression

$$\left\{ \begin{array}{l} e^{-\frac{\Delta t}{2}\mathbf{S}} \approx R_{rq} \left(-\frac{\Delta t}{2}\mathbf{S} \right) = \frac{N_{rq} \left(-\frac{\Delta t}{2}\mathbf{S} \right)}{D_{rq} \left(-\frac{\Delta t}{2}\mathbf{S} \right)}, \\ N_{rq} \left(-\frac{\Delta t}{2}\mathbf{S} \right) = \sum_{k=0}^r \frac{(r+q-k)! r!}{(r+q)! k! (r-k)!} \left(-\frac{\Delta t}{2}\mathbf{S} \right)^k, \\ D_{rq} \left(-\frac{\Delta t}{2}\mathbf{S} \right) = \sum_{k=0}^q \frac{(r+q-k)! q!}{(r+q)! k! (r-k)!} \left(\frac{\Delta t}{2}\mathbf{S} \right)^k. \end{array} \right. \quad (46)$$

In the following numerical experiments, the parameters $r = q = 6$ are used.

It remains to verify that the numerical integration of the diffusive step (45) is unconditionally stable. This is achieved as follows.

Proposition 3. *The diffusive part of the splitting (42) is well-posed whatever the weights a_ℓ in the diffusive approximation (24).*

Proposition 3 is proven in appendix 2. It follows that the solution of system (B.1) is bounded and that the eigenvalues of $-\frac{\Delta t}{2}\mathbf{S}$ are then in the left half space. As a consequence, the R_{qq} Padé approximation is always stable [28]. The full algorithm (43) is therefore stable under the optimum stability condition

$$\Delta t \leq \Upsilon \frac{\Delta x}{c_{pf}^\infty}, \quad (47)$$

which is always independent of the Biot-DA model coefficients.

5. Numerical experiments

5.1. General configuration

Saturating fluid	ρ_f (kg/m ³)	1000
	η (Pa.s)	10^{-3}
Grain	ρ_s (kg/m ³)	2644
	μ (Pa)	$7.04 \cdot 10^9$
Matrix	ϕ	0.2
	a	2.4
	κ (m ²)	$3.6 \cdot 10^{-13}$
	λ_f (Pa)	$1.06 \cdot 10^{10}$
	m (Pa)	$9.70 \cdot 10^9$
	β	0.720
	Λ (m)	$5.88 \cdot 10^{-6}$
	Phase velocities	c_{pf}^∞ (m/s)
c_{ps}^∞ (m/s)		814.95
$c_{pf}^\infty/c_{ps}^\infty$		4.01
f_c (Hz)		$3.68 \cdot 10^4$

Table 2: Physical parameters used in numerical experiments.

The physical parameters used in all the numerical experiments, which are given in table 2, correspond to Berea sandstone saturated with water. Truncated values of the parameters are given: in particular, the viscous characteristic length Λ corresponds rigorously to a Pride number $P = 0.5$ (6). The unbounded medium is excited by a point source $f_\sigma = g(t)h(x)$, with $h(x) = \delta(x)$ in equation (11c). The time-dependent evolution of the source, $g(t)$ in (11c), is a C^6 combination of truncated sinusoids

$$g(t) = \begin{cases} \sin(\omega_0 t) - \frac{21}{32} \sin(2\omega_0 t) + \frac{63}{768} \sin(4\omega_0 t) - \frac{1}{512} \sin(8\omega_0 t) & \text{if } 0 \leq t \leq \frac{1}{f_0}, \\ 0 & \text{otherwise,} \end{cases} \quad (48)$$

with a central frequency $f_0 = \frac{\omega_0}{2\pi} = 200$ kHz. Adopting the high-frequency regime is therefore completely justified since $f_0 \simeq 5 \times f_c$. Figure 5 shows the time-dependent evolution and spectrum of the source.

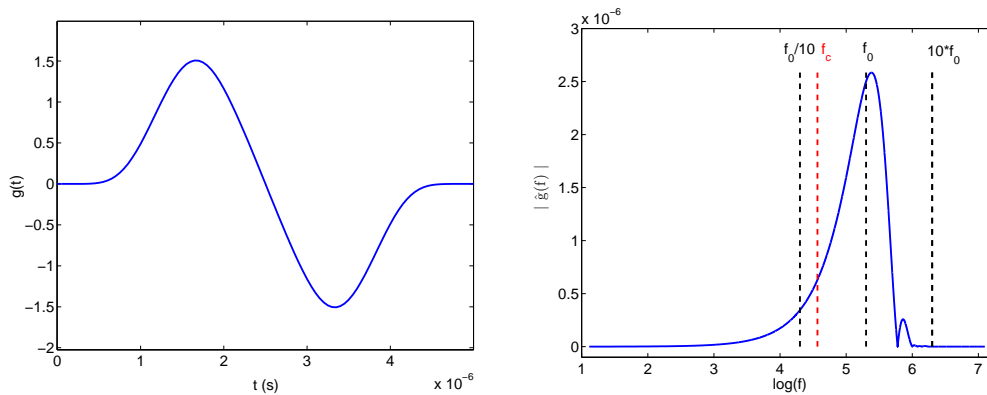


Figure 5: Time-dependent evolution (left) and spectrum (right) of the source.

The computational domain $[-0.04, 0.04]$ m is discretized with N_x grid points, and the time step is deduced from (47), taking $\Upsilon = 0.9$. No special care is applied to simulate outgoing waves (with PML, for instance), since the simulations are stopped before the waves have reached the edges of the computational domain. The numerical experiments are performed on an Intel Core i7 processor at 2.80 GHz.

Exact solutions of time-domain Biot-JKD equations have been derived in the literature [13], but not for Biot-DA. Therefore, we compute reference solutions of both Biot-JKD and Biot-DA thanks to standard tools of Fourier analysis: the Green functions of (11) or (26) are determined in the harmonic regime. Then, the Cauchy residue theorem and numerical inverse Fourier transforms ($N_f = 9.6 \cdot 10^5$ modes and a frequency step $\Delta f \simeq 13$ Hz) yield the semi-analytical solutions.

5.2. Test 1: Biot-DA

The aim of this first test is to check the validity of the numerical method presented above using Biot-DA model. The domain is discretized with $N_x = 700$ which amounts to 32 points per slow wavelength and 142 points per fast wavelength, and $N = 6$ diffusive variables are used. The source point emits symmetrically rightward and leftward moving fast and slow compressional

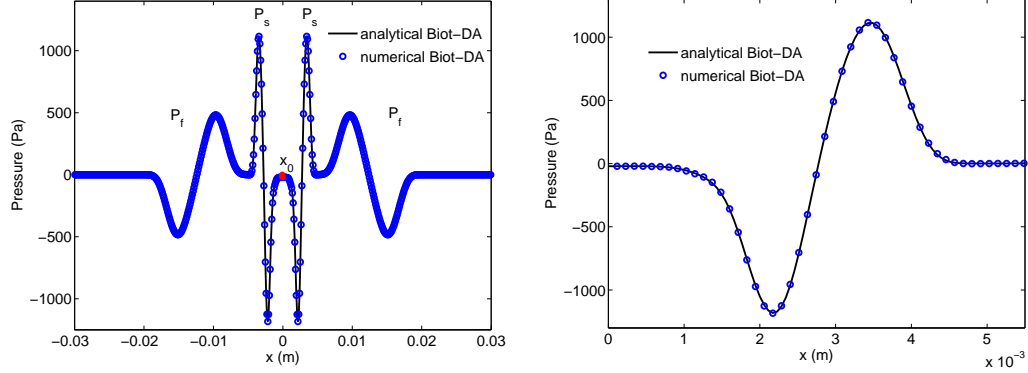


Figure 6: Test 1. Fast waves P_f and slow waves P_s emitted by a source point at $x_0 = 0$ m. Comparison between numerical values (circle) and Biot-DA analytical values (solid line) of p at $t_1 \simeq 6.29 \cdot 10^{-6}$ s. Right: zoom on the slow wave.

waves, which are denoted P_f and P_s , respectively, in figure 6. It can be seen from this figure that the numerical and analytical values of the pressure after 200 time steps show excellent agreement.

The error between the exact and numerical solutions will be measured in the L_2 norm in the domain $[-0.04, 0.04]$ m at time $t_1 \simeq 6.29 \cdot 10^{-6}$ s. Numerical values of the relative error and convergence order are summed up in table 3 at various values of N_x and given in figure 7-(a). The convergence rate obtained by performing a linear regression is 1.97818, which is very similar to the theoretical second-order of the global algorithm.

Figure 7-(b) shows the computational time in terms of the number of diffusive variables N , with $N_x = 700$. The complexity of the scheme in term of diffusive variables is found to be in $\mathcal{O}(N^2)$.

With $N = 6$ diffusive variables, the linear optimization procedure described in section 3.3 yields: $a_1 = -371.44$, $a_2 = 2332.78$, $a_3 = -3109.17$, $a_4 = 4506.03$, $a_5 = -4524.14$ and $a_6 = 7096.95$. Since some of the coefficients are negative, one cannot confirm that E is a decreasing energy in proposition 2. To examine this question numerically, the time evolution of E_3 in (33) and $-dE/dt$ in (34) is shown in figure 8, where it can be seen that $E_3 > 0$, hence $E > 0$, and that $dE/dt < 0$. Despite the negativity of some a_ℓ , figure 8 indicates that E is a decreasing energy and that Biot-DA is a well-posed problem.

N_x	Error L_2	Order
1000	$1.660 \cdot 10^{-1}$	-
2000	$1.554 \cdot 10^{-2}$	3.417
3000	$5.939 \cdot 10^{-3}$	2.372
4000	$3.300 \cdot 10^{-3}$	2.043
5000	$2.121 \cdot 10^{-3}$	1.981
6000	$1.482 \cdot 10^{-3}$	1.968
7000	$1.095 \cdot 10^{-3}$	1.963
8000	$8.428 \cdot 10^{-4}$	1.958
9000	$6.699 \cdot 10^{-4}$	1.950
10000	$5.462 \cdot 10^{-4}$	1.937

Table 3: Test 1: error measurements and convergence orders.

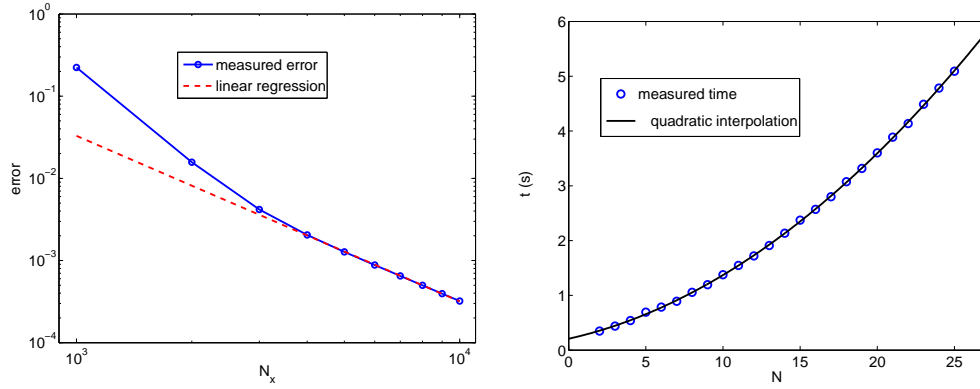


Figure 7: Test 1: relative error between exact and numerical solutions (left) in terms of the number of grid nodes N_x . The dashed line is proportional to N_x^{-2} . CPU time (right) in terms of the number of diffusive variables N .

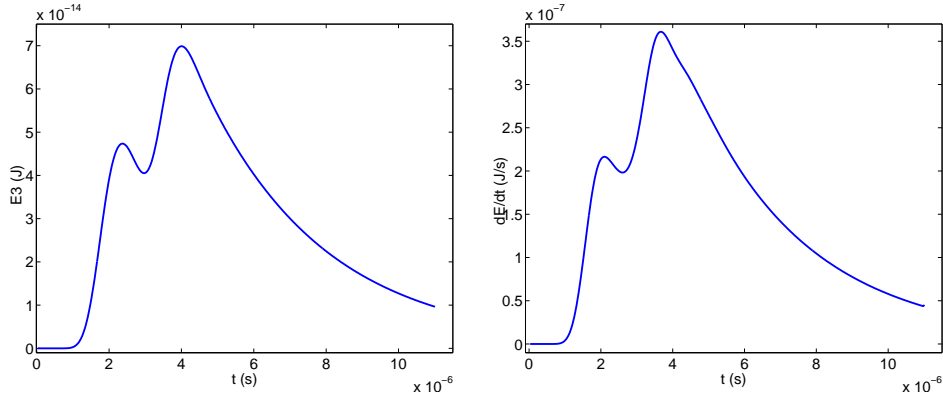


Figure 8: Test1. Left: time-dependent evolution of E_3 (33); right: time-dependent evolution of $-dE/dt$ (34).

5.3. Test 2: Biot-JKD

The aim of the second test is to check the validity of the mathematical and numerical methods used to approximate the physical Biot-JKD model. Figure 9 compares the numerical pressure obtained with the Biot-DA model with the analytical pressure obtained with the Biot-JKD model, at times t_1 and $t_2 > t_1$. The dispersion and attenuation of the slow wave can be clearly observed. Excellent agreement is found to exist between the two solutions.

Two errors should be mentioned here: the modeling error ε_m , defined as the difference between the Biot-DA and Biot-JKD models; and the numerical error, ε_n , resulting from the numerical discretization of the Biot-DA model. The total error ε_t obviously satisfies:

$$\varepsilon_t \leq \varepsilon_m + \varepsilon_n. \quad (49)$$

Based on section 3.3, taking $N = 6$ yields $\varepsilon_m = 5.48\%$. In test 1, $\varepsilon_n \simeq 1.70\%$ was measured. At t_1 , the total error $\varepsilon_t = 1.95\%$, which means that the inequality (49) is satisfied but not optimally: the overall results are more accurate than those predicted on the basis of the bound (49). The results of this test confirm that the method presented above efficiently approximates the transient waves modeled by the Biot-JKD model.

5.4. Test 3: variable medium

The aim of the third test is to establish whether the numerical methods presented in this paper can be used to handle more complex media. As an

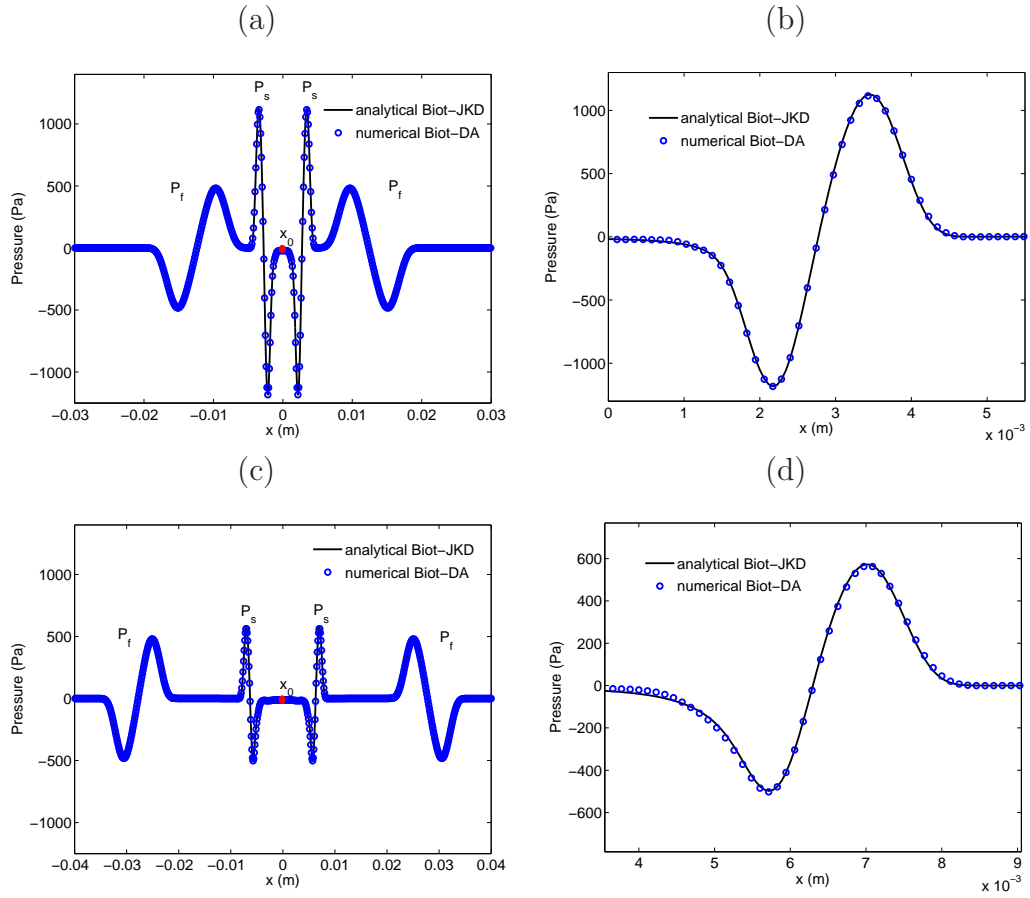


Figure 9: Test 2. Fast waves P_f and slow waves P_s emitted by a source point at $t_1 \simeq 6.29 \cdot 10^{-6}$ s (a-b) and $t_2 \simeq 1.10 \cdot 10^{-5}$ s (c-d). Comparison between the numerical Biot-DA pressure (circle) and the exact Biot-JKD pressure (solid line). Right row: zoom on the slow wave.

example, we took the porous medium with the parameters defined in table 2, except for the ratio η/κ , which varies linearly from $1.5 \cdot 10^4 \text{ Pa}\cdot\text{s}\cdot\text{m}^{-2}$ at $x = -0.04 \text{ m}$ to $5 \cdot 10^9 \text{ Pa}\cdot\text{s}\cdot\text{m}^{-2}$ at $x = 0.04 \text{ m}$. These values are purely numerical and are not based on real data. Some changes had to be made to the method in comparison with that used in the homogeneous case:

- at a given level of accuracy ε_m , the most-penalizing number of diffusive variables N has to be determined;
- the coefficients a_ℓ have to be computed and stored at each grid point.

In (29), the diffusive matrix \mathbf{S} therefore differs between the grid points. In this example, the propagation matrix \mathbf{A} remains unchanged since only the diffusive part is modified. When dealing with a real continuously variable medium, which occurs in the case of many applications [15], the present ADER scheme would also have to be modified in order to handle the spatial changes in the matrix \mathbf{A} accurately.

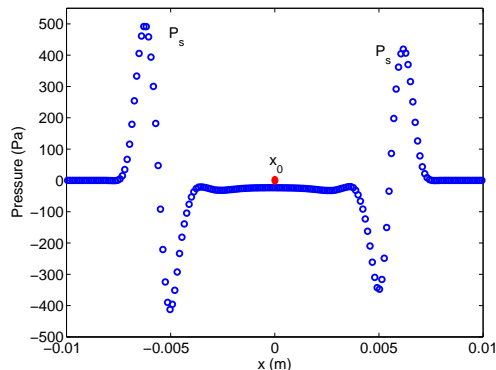


Figure 10: Test 3. Pressure at $t_1 \simeq 6.29 \cdot 10^{-6} \text{ s}$ (zoom on the slow wave).

Figure (10) shows the pressure p at $t_1 \simeq 6.29 \cdot 10^{-6} \text{ s}$. As was to be expected, the rightward-moving slow wave is more strongly attenuated than the leftward-moving one, because the values of η/κ are higher in the right part of the domain. The present numerical tool therefore provides useful means for computing solutions of this kind, where no analytical expressions are available.

5.5. Test 4: a 2-D example

The one-dimensional method presented here can easily be extended to other dimensions. As a preliminary example, we take a two-dimensional medium with the parameters given in table 2. The number of physical unknowns increase in this case from 4 to 8, and the equations of motion are also written in the form of a first-order hyperbolic linear system. The propagative part is solved with the ADER 4 numerical scheme. The diffusive part involves an order 1/2 fractional derivative for each component of the filtration velocity. The computational domain is set at $[-0.08, 0.08]^2$ m. A Ricker source point, with a central frequency of 200 kHz and a time shift 10^{-5} s, is localized at point (0,0) and applied to the σ_{xy} component of the stress tensor. Applying our method with $N = 6$ diffusive variables to a grid of $N_x = N_y = 1400$ points gives the results presented in figure 11. Fast and slow compressional waves are observed as regards the pressure, while the additional shear wave is present in the σ_{xx} component of the stress tensor. It is proposed in future studies to address the analytical solution of the 2D Biot-JKD model and to perform an error analysis of the results obtained with the Biot-DA model.

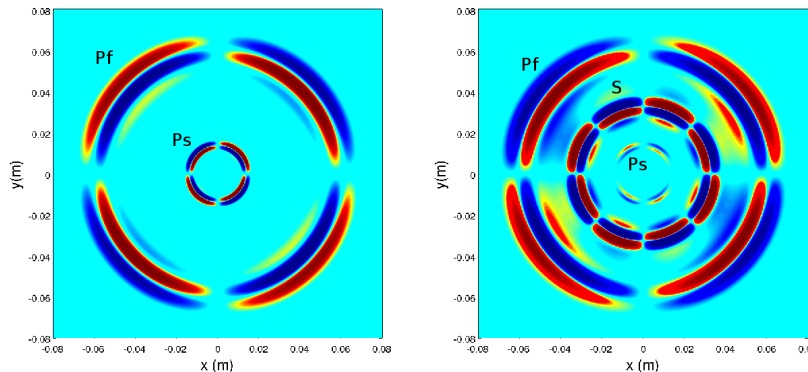


Figure 11: Test 4. Graph of the pressure (left) and the stress component σ_{xx} (right) emitted by a source point, at time $t = 2.32 \cdot 10^{-5}$ s.

6. Conclusion

A numerical method is presented here for simulating transient poroelastic waves in the high-frequency range. The Biot-JKD model, which involves or-

der $1/2$ fractional derivatives, was replaced here by an approximate Biot-DA model, which is much more tractable numerically. Contrary to the approach used in [25], the Biot-DA coefficients are determined here using an optimization procedure, which depends on the frequency range of interest. The number of parameters and the accuracy of the model were quantified. The hyperbolic system of partial differential equations was discretized using efficient tools (Strang splitting and the fourth-order ADER scheme). The stability condition of the numerical scheme is always independent of the parameters involved in the approximate Biot-DA model. Numerical experiments performed in some academic cases (1-D homogeneous media) confirmed the reliability of this approach, and some preliminary simulations (with variable media, or in the 2-D context) show that the method is applicable to complex media.

Some suggestions for future lines of research:

- *Thermic boundary-layer.* In cases where the saturating fluid is a gas, thermo-mechanical effects have to be taken into account. Extended versions of the Biot-JKD have been developed [20], involving additional order $1/2$ fractional derivatives. The numerical method developed in this paper should lend itself well to working with this model.
- *Slow shear wave.* A poroelastic theory that accounts properly for the fluid shear stress relaxation has been recently proposed [29, 30], predicting the existence of a slow shear wave. This additional mode is heavily damped far from the source, but it can play a key role in balance equations near interfaces, as the slow compressional wave. To our knowledge, no time-domain simulations of this model have been proposed so far.
- *Heterogeneous porous media.* Methods of modeling material interfaces in the context of Cartesian grids have been previously developed, based on an immersed interface method [23]. The possibility of applying this method to porous media in the low frequency range was studied in [6, 7, 8, 21]. Work on means of extending this method to the Biot-JKD model is currently in progress.

Acknowledgments

We are grateful to Denis Matignon (ISAE, Toulouse) for fruitful discussions about fractional derivatives. We also thank Zine Fellah, Erick Ogam,

Armand Wirgin (LMA, Marseille), Gaëlle Lefeuvre-Mesgouez and Arnaud Mesgouez (EMMAH, Avignon) for their careful reading of the manuscript.

Appendix A. Proof of proposition 1

The equation (9a) is multiplied by v_s and integrated

$$\int_{\mathbb{R}} \left(\rho v_s \frac{\partial v_s}{\partial t} + \rho_f v_s \frac{\partial w}{\partial t} - v_s \frac{\partial \sigma}{\partial x} \right) dx = 0. \quad (\text{A.1})$$

The first term in (A.1) is written

$$\int_{\mathbb{R}} \rho v_s \frac{\partial v_s}{\partial t} dx = \frac{d}{dt} \frac{1}{2} \int_{\mathbb{R}} \rho v_s^2 dx. \quad (\text{A.2})$$

Integrating by part and using (9d), we obtain

$$\begin{aligned} - \int_{\mathbb{R}} v_s \frac{\partial \sigma}{\partial x} dx &= \int_{\mathbb{R}} \frac{\partial v_s}{\partial x} \sigma dx, \\ &= \int_{\mathbb{R}} \frac{\partial \varepsilon}{\partial t} (C \varepsilon - \beta p) dx, \\ &= \int_{\mathbb{R}} C \varepsilon \frac{\partial \varepsilon}{\partial t} dx - \int_{\mathbb{R}} \beta p \frac{\partial \varepsilon}{\partial t} dx, \\ &= \frac{d}{dt} \frac{1}{2} \int_{\mathbb{R}} C \varepsilon^2 dx - \int_{\mathbb{R}} \beta p \frac{\partial \varepsilon}{\partial t} dx, \\ &= \frac{d}{dt} \left(\frac{1}{2} \int_{\mathbb{R}} \frac{1}{C} (\sigma + \beta p)^2 dx \right) - \int_{\mathbb{R}} \beta p \frac{\partial \varepsilon}{\partial t} dx. \end{aligned} \quad (\text{A.3})$$

The equation (9b) is multiplied by w and integrated

$$\int_{\mathbb{R}} \left(\rho_f w \frac{\partial v_s}{\partial t} + \rho_w w \frac{\partial w}{\partial t} + \frac{\eta}{\kappa} \frac{1}{\sqrt{\Omega}} w (D + \Omega)^{1/2} w + w \frac{\partial p}{\partial x} \right) dx = 0. \quad (\text{A.4})$$

The second term in (A.4) can be written

$$\int_{\mathbb{R}} \rho_w w \frac{\partial w}{\partial t} dx = \frac{d}{dt} \frac{1}{2} \int_{\mathbb{R}} \rho_w w^2 dx. \quad (\text{A.5})$$

Integrating by part and using (9d), we obtain

$$\begin{aligned}
\int_{\mathbb{R}} w \frac{\partial p}{\partial x} dx &= - \int_{\mathbb{R}} p \frac{\partial w}{\partial x} dx, \\
&= \int_{\mathbb{R}} p \frac{\partial \xi}{\partial t} dx, \\
&= \int_{\mathbb{R}} p \frac{\partial}{\partial t} \left(\frac{1}{m} p + \beta \varepsilon \right) dx, \\
&= \int_{\mathbb{R}} \frac{1}{m} p \frac{\partial p}{\partial t} dx + \int_{\mathbb{R}} \beta p \frac{\partial \varepsilon}{\partial t} dx, \\
&= \frac{d}{dt} \left(\frac{1}{2} \int_{\mathbb{R}} \frac{1}{m} p^2 dx \right) + \int_{\mathbb{R}} \beta p \frac{\partial \varepsilon}{\partial t} dx.
\end{aligned} \tag{A.6}$$

After adding (A.1) and the first term in (A.4), there remains

$$\int_{\mathbb{R}} \rho_f \left(v_s \frac{\partial w}{\partial t} + w \frac{\partial v_s}{\partial t} \right) dx = \frac{d}{dt} \int_{\mathbb{R}} \rho_f v_s w dx. \tag{A.7}$$

Equations (A.1)-(A.4) and the diffusive representation (15) yield

$$\frac{d}{dt} (E_1 + E_2) = - \int_{\mathbb{R}} \int_{\theta \in \mathbb{R}^+} \frac{\eta}{\kappa} \frac{1}{\pi} \frac{1}{\sqrt{\Omega \theta}} w \psi d\theta dx. \tag{A.8}$$

To calculate the right-hand side of (A.8), equation (17) is multiplied by w or ψ

$$\begin{cases} w \frac{\partial \psi}{\partial t} - w \frac{\partial w}{\partial t} + (\theta + \Omega) w \psi - \Omega w^2 = 0, \end{cases} \tag{A.9a}$$

$$\begin{cases} \psi \frac{\partial \psi}{\partial t} - \psi \frac{\partial w}{\partial t} + (\theta + \Omega) \psi^2 - \Omega w \psi = 0. \end{cases} \tag{A.9b}$$

After performing some algebraic operations on (A.9b), (A.9a) and (A.8), one easily obtains the relation (19). It remains to prove that E is a positive definite quadratic form. This is obviously so for E_2 and E_3 . Concerning E_1 , we write

$$\begin{aligned}
\Delta &= \frac{1}{2} \rho v_s^2 + \frac{1}{2} \rho_w w^2 + \rho_f v_s w, \\
&= \frac{1}{2} \mathbf{X}^T \mathbf{H} \mathbf{X},
\end{aligned} \tag{A.10}$$

where

$$\mathbf{X} = \begin{pmatrix} v_s \\ w \end{pmatrix} \quad \mathbf{H} = \begin{pmatrix} \rho & \rho_f \\ \rho_f & \rho_w \end{pmatrix}. \quad (\text{A.11})$$

Taking \mathcal{S} and \mathcal{P} to denote the sum and the product of the eigenvalues of matrix \mathbf{H} , we obtain

$$\begin{aligned} \mathcal{P} &= \det \mathbf{H} = \rho \rho_w - \rho_f^2 = \chi > 0, \\ \mathcal{S} &= \text{Tr} \mathbf{H} = \rho + \rho_w > 0. \end{aligned} \quad (\text{A.12})$$

The two eigenvalues of \mathbf{H} are therefore positive, which proves that Δ is definite positive and completes the proof.

Appendix B. Proof of proposition 3

From (26), the system of diffusive evolution equations writes

$$\begin{cases} \frac{\partial v_s}{\partial t} = \frac{\rho_f}{\rho} \gamma \sum_{\ell=1}^N a_\ell \psi_\ell, & (\text{B.1a}) \end{cases}$$

$$\begin{cases} \frac{\partial w}{\partial t} = -\gamma \sum_{\ell=1}^N a_\ell \psi_\ell, & (\text{B.1b}) \end{cases}$$

$$\begin{cases} \frac{\partial \sigma}{\partial t} = 0, & (\text{B.1c}) \end{cases}$$

$$\begin{cases} \frac{\partial p}{\partial t} = 0, & (\text{B.1d}) \end{cases}$$

$$\begin{cases} \frac{\partial \psi_j}{\partial t} = \Omega w - \gamma \sum_{\ell=1}^N a_\ell \psi_\ell - (\theta_j + \Omega) \psi_j, \quad j = 1, \dots, N. & (\text{B.1e}) \end{cases}$$

Equation (B.1b) is multiplied by w and (B.1e) is multiplied by ψ_j

$$\begin{cases} w \frac{\partial w}{\partial t} = -\gamma w \sum_{\ell=1}^N a_\ell \psi_\ell, & (\text{B.2a}) \end{cases}$$

$$\begin{cases} \psi_j \frac{\partial \psi_j}{\partial t} = \Omega w \psi_j - \gamma \psi_j \sum_{\ell=1}^N a_\ell \psi_\ell - (\theta_j + \Omega) \psi_j^2, \quad j = 1, \dots, N. & (\text{B.2b}) \end{cases}$$

Summing (B.2a) and (B.2b) gives

$$w \frac{\partial w}{\partial t} + \psi_j \frac{\partial \psi_j}{\partial t} = \Omega w \psi_j - (\theta_j + \Omega) \psi_j^2 - \gamma (w + \psi_j) \sum_{\ell=1}^N a_\ell \psi_\ell, \quad j = 1, \dots, N. \quad (\text{B.3})$$

The left-hand-side of (B.3) is equal to $\frac{d}{dt} \frac{1}{2} (w^2 + \psi_j^2)$. Then (B.1b) is multiplied by ψ_j and (B.1e) is multiplied by w

$$\begin{cases} \psi_j \frac{\partial w}{\partial t} = -\gamma \psi_j \sum_{\ell=1}^N a_\ell \psi_\ell, & j = 1, \dots, N, \\ w \frac{\partial \psi_j}{\partial t} = \Omega w^2 - \gamma w \sum_{\ell=1}^N a_\ell \psi_\ell - (\theta_j + \Omega) w \psi_j, & j = 1, \dots, N \end{cases} \quad (\text{B.4a})$$

Summing (B.4a) and (B.4b) gives

$$w \frac{\partial \psi_j}{\partial t} + \psi_j \frac{\partial w}{\partial t} = \Omega w^2 - (\theta_j + \Omega) w \psi_j - \gamma (w + \psi_j) \sum_{\ell=1}^N a_\ell \psi_\ell, \quad j = 1, \dots, N. \quad (\text{B.5})$$

The left-hand-side of (B.5) writes $\frac{\partial}{\partial t} (w \psi_j)$. Elementary calculations on (B.5) and (B.3) yield ($j = 1, \dots, N$)

$$\frac{d}{dt} \left(\frac{1}{2} (w^2 + \psi_j^2) - w \psi_j \right) = - (\Omega w^2 - (\theta_j + 2\Omega) w \psi_j + (\theta_j + \Omega) \psi_j^2). \quad (\text{B.6})$$

Taking

$$\begin{cases} E_j &= \frac{1}{2} (w - \psi_j)^2 > 0, \\ E &= \sum_{j=1}^N E_j > 0, \\ \mathbf{X}_j &= \begin{pmatrix} w \\ \psi_j \end{pmatrix} \\ \mathbf{H}_j &= \begin{pmatrix} \Omega & -(\theta_j + 2\Omega) \\ 0 & \theta_j + \Omega \end{pmatrix}, \end{cases} \quad (\text{B.7})$$

and summing the relations (B.6) for $j = 1, \dots, N$ yields

$$\frac{dE}{dt} = - \sum_{j=1}^N \mathbf{X}_j^T \mathbf{H}_j \mathbf{X}_j. \quad (\text{B.8})$$

Since the matrix \mathbf{H}_j is triangular, its two eigenvalues are $\Omega > 0$ and $\theta_j + \Omega > 0$. The quadratic form $\mathbf{X}_j^T \mathbf{H}_j \mathbf{X}_j$ is therefore definite and positive, which means that the left-hand-side of (B.8) is strictly negative. The energy E derived from system (B.1) is therefore decreasing, and hence the system (B.1) is well-posed.

References

- [1] M. A. BIOT, *Theory of propagation of elastic waves in a fluid-saturated porous solid. I: Low-frequency range*, J. Acoust. Soc. Am., 28-2 (1956), 168-178.
- [2] M. A. BIOT, *Theory of propagation of elastic waves in a fluid-saturated porous solid. II: High-frequency range*, J. Acoust. Soc. Am., 28-2 (1956), 179-191.
- [3] T. BOURBIÉ, O. COUSSY, B. ZINSZNER, *Acoustics of Porous Media*, Gulf Publishing Company (1987).
- [4] J.M. CARCIONE, *Wave Fields in Real Media: Wave Propagation in Anisotropic, Anelastic, Porous and Electromagnetic Media*, Elsevier, 2007.
- [5] J.M. CARCIONE, C. MORENCY, J.E. SANTOS, *Computational poroelasticity - A review*, Geophysics, 75-5 (2010), 75A229-75A243.
- [6] G. CHIAVASSA, B. LOMBARD, J. PIRAUX, *Numerical modeling of 1-D transient poroelastic waves in the low-frequency range*, J. Comput. Appl. Math., 234-6 (2010), 1757-1765.
- [7] G. CHIAVASSA, B. LOMBARD, *Time domain numerical modeling of wave propagation in 2D heterogeneous porous media*, J. Comput. Phys., 230-13 (2011), 5288-5309.
- [8] G. CHIAVASSA, B. LOMBARD, *Wave propagation across acoustic /Biot's media: a finite-difference method*, Commun. Comput. Phys., in press (2012).
- [9] W. DESCH, R. MILLER, *Exponential stabilization of Volterra integral equations with singular kernels*, J. Integral Equations Appl., 1-3 (1988), 397-433.

- [10] F. DUBOIS, A. GALUCIO, N. POINT, *Introduction à la dérivation fractionnaire : théorie et applications*, (2010), <http://www.math.u-psud.fr/~fdubois>.
- [11] H. EMMERICH, M. KORN, *Incorporation of attenuation into time-domain computations of seismic wave fields*, *Geophysics*, 52-9 (1987), 1252-1264.
- [12] A. EZZIANI, *Modélisation mathématique et numérique de la propagation d'ondes dans les milieux viscoélastiques et poroélastiques*, PhD thesis, Université Paris Dauphine, France (2005).
- [13] Z. E. A. FELLAH, J. Y. CHAPELON, S. BERGER, W. LAURIKS, C. DEPOLIER, *Ultrasonic wave propagation in human cancellous bone: application of Biot theory*, *J. Acoust. Soc. Am.*, 116-1 (2004), 61-73.
- [14] B.P. FLANNERY, W.H. PRESS, S.A. TEUKOLSKY, W.T. VETTERLING, *Numerical Recipes in C: the Art of Scientific Computing*, Second Edition, Cambridge University Press (1992).
- [15] G. GAUTIER, J. P. GROBY, O. DAZEL, L. KELDERS, L. DE RYCK, P. LECLAIRE, *Propagation of acoustic waves in a one-dimensional macroscopically inhomogeneous poroelastic material*, *J. Acoust. Soc. Am.*, 130 (2011), 1390-1398.
- [16] J.P. GROBY, C. TSOGKA, *A time domain method for modeling viscoacoustic wave propagation*, *J. Comput. Acoust.*, 14-2 (2006), 201-236.
- [17] H. HADDAR, J.R. LI, D. MATIGNON, *Efficient solution of a wave equation with fractional-order dissipative terms*, *J. Comput. Appl. Math.*, 234-6 (2010), 2003-2010.
- [18] D. HELESCHWITZ, *Analyse et simulation de systeme différentiels fractionnaires et pseudo-différentiels linéaires sous représentation diffusive*, PhD thesis, ENST, France (2000).
- [19] D.L. JOHNSON, J. KOPLIK, R. DASHEN, *Theory of dynamic permeability and tortuosity in fluid-saturated porous media*, *J. Fluid Mech.*, 176 (1987), 379-402.

- [20] D. LAFARGE, P. LEMARINIER, J.F. ALLARD, *Dynamic compressibility of air in porous structures at audible frequencies*, J. Acoust. Soc. Am, 102-4 (1997), 1995-2005.
- [21] G. LEFEUVE-MESGOUEZ, A. MESGOUEZ, G. CHIAVASSA, B. LOMBARD, *Semi-analytical and numerical methods for computing transient waves in 2D acoustic / poroelastic stratified media*, Wave Motion, 49 (2012), 667-680.
- [22] R. J. LEVEQUE, *Finite Volume Methods for Hyperbolic Problems*, Cambridge University Press (2002).
- [23] B. LOMBARD, J. PIRAUX, *Numerical treatment of two-dimensional interfaces for acoustic and elastic waves*, J. Comput. Phys., 195-1 (2004), 90-116.
- [24] B. LOMBARD, J. PIRAUX, *Numerical modeling of transient two-dimensional viscoelastic waves*, J. Comput. Phys., 230-15 (2011), 6099-6114.
- [25] J.F. LU, A. HANYGA, *Wave field simulation for heterogeneous porous media with singular memory drag force*, J. Comput. Phys., 208-2 (2005), 651-674.
- [26] C. LUBICH, *Discretized fractional calculus*, SIAM J. Math. Anal., 17 (1986), 704-719.
- [27] Y.J. MASSON, S.R. PRIDE, *Finite-difference modeling of Biot's poroelastic equations across all frequencies*, Geophysics, 75-2 (2010), N33-N41.
- [28] C. B. MOLER, C. F. VAN LOAN, *Nineteen dubious ways to compute the exponential of a matrix, twenty-five years later*, SIAM Review, 45 (2003), 3-49.
- [29] T. M. MÜLLER, P. N. SAHAY, *Fast compressional wave attenuation and dispersion due to conversion scattering into slow shear waves in randomly heterogeneous porous media*, J. Acoust. Soc. Am., 129-5 (2011), 2785-2796.

- [30] T. M. MÜLLER, P. N. SAHAY, *Stochastic theory of dynamic permeability in poroelastic media*, Physical Review E 84 (2011), 026329.
- [31] J. NOCEDAL, S. J. WRIGHT, *Numerical Optimization*, Springer (1999).
- [32] T. J. PLONA, *Observation of a second bulk compressional wave in a porous medium at ultrasonic frequencies*, Appl. Phys. Lett., 36-4 (1980), 259-261.
- [33] T. SCHWARTZKOPFF, M. DUMBSER, C. MUNZ, *Fast high order ADER schemes for linear hyperbolic equations*, J. Comput. Phys., 197-2 (2004), 532-539.
- [34] N. SEBAA, Z. E. A. FELLAH, M. FELLAH, E. OGAM, A. WIRGIN, F. G. MITRI, C. DEPOLLIER, W. LAURIKS, *Ultrasonic characterization of human cancellous bone using the Biot theory: inverse problem*, J. Acoust. Soc. Am., 120-4 (2006), 1816-1824.
- [35] O. J. STAFFANS, *Well-posedness and stabilizability of a viscoelastic equation in energy space*, Trans. Amer. Math. Soc., 345-2 (1994), 527-575.
- [36] F. TORRES, P. VAUDON, B. JECKO, *Application of fractional derivatives to the FDTD modeling of pulse propagation in a Cole-Cole dispersive medium*, Microwave Opt. Technol. Lett., 13-5 (1996), 300-304.